TU Delft

Delft University of Technology

Lifetime Prediction of Current-and Temperature-Induced Degradation in Silicone-Encapsulated 365 nm High-Power Light-Emitting Diodes

Herzog, Alexander ; Benkner, Simon ; Zandi, Babak; Buffolo, Matteo; van Driel, Willem D.; Meneghini, Matteo; Khanh, Tran Quoc

DOI
10.1109/ACCESS.2023.3249478

Publication date
2023

Document Version
Final published version

Published in
IEEE Access

Citation (APA)
Herzog, A., Benkner, S., Zandi, B., Buffolo, M., van Driel, W. D., Meneghini, M., & Khanh, T. Q. (2023). Lifetime Prediction of Current-and Temperature-Induced Degradation in Silicone-Encapsulated 365 nm High-Power Light-Emitting Diodes. *IEEE Access*, *11*, 19928-19940. https://doi.org/10.1109/ACCESS.2023.3249478

Important note
To cite this publication, please use the final published version (if applicable).
Please check the document version above.

Copyright
Other than for strictly personal use, it is not permitted to download, forward or distribute the text or part of it, without the consent of the author(s) and/or copyright holder(s), unless the work is under an open content license such as Creative Commons.

Takedown policy
Please contact us and provide details if you believe this document breaches copyrights.
We will remove access to the work immediately and investigate your claim.

This work is downloaded from Delft University of Technology.
For technical reasons the number of authors shown on this cover page is limited to a maximum of 10.

IEEE Access
Multidisciplinary | Rapid Review | Open Access Journal

Received 31 January 2023, accepted 22 February 2023, date of publication 27 February 2023, date of current version 2 March 2023.

Digital Object Identifier 10.1109/ACCESS.2023.3249478

RESEARCH ARTICLE

Lifetime Prediction of Current- and Temperature-Induced Degradation in Silicone-Encapsulated 365 nm High-Power Light-Emitting Diodes

ALEXANDER HERZOG [1], SIMON BENKNER [1], BABAK ZANDI [1], MATTEO BUFFOLO [2], (Associate Member, IEEE), WILLEM D. VAN DRIEL [3,4], MATTEO MENEGHINI [2], (Senior Member, IEEE), AND TRAN QUOC KHANH [1]

[1]Laboratory of Adaptive Lighting Systems and Visual Processing, Technische Universität Darmstadt, 64289 Darmstadt, Germany
[2]Department of Electrical Engineering, University of Padova, 35131 Padova, Italy
[3]EEMCS Faculty, Delft University of Technology, 2628 CD Delft, The Netherlands
[4]Signify, 5656 AE Eindhoven, The Netherlands

Corresponding author: Alexander Herzog (herzog@lichttechnik.tu-darmstadt.de)

This work was supported by the ECSEL Joint Undertaking (JU) through the European Union's Horizon 2020 Research and Innovation Program by The Netherlands, Hungary, France, Poland, Austria, Germany, Italy, Switzerland, under Agreement 101007319.

ABSTRACT We report on the degradation mechanisms and dynamics of silicone encapsulated ultraviolet A (UV-A) high-power light-emitting diodes (LEDs), with a peak wavelength of 365 nm. The stress tests were carried out for a period of 8665 hours with forward currents between 350 mA and 700 mA and junction temperatures up to 132 °C. Depending on stress condition, a significant decrease in optical power could be observed, being accelerated with higher operating conditions. Devices stressed at a case temperature of 55 °C indicate a decrease in radiant flux between 10 - 40 % varying with measurement current, whereas samples stressed at higher case temperatures exhibit crack formation in the silicone encapsulant accompanied by electromigration shorting the active region. The analyzed current and temperature dependency of the degradation mechanisms allows to propose a degradation model to determine the device lifetime at different operating parameters. Additional stress test data collected at different aging conditions is used to validate the model's lifetime predictions.

INDEX TERMS Light-emitting diode (LED), degradation, UV-A, lifetime prediction, reliability, lens cracking, silicone lens, ultraviolet.

I. INTRODUCTION

Due to the steady development of GaN-based semiconductor light sources, conventional light sources of the visible spectral range are already replaced by semiconductor light sources in various applications. Whereas LEDs of the blue spectral range have an electro-optical efficiency of up to 80 % and offer an alternative to conventional light sources in combination with appropriate phosphors, the efficiency of emitters in the ultraviolet spectral range diminishes significantly [1], [2]. Therefore, conventional radiation sources can only be replaced by ultraviolet semiconductor emitters to a limited extent. The reduced efficiency of UV emitters is due to both, the semiconductor materials used and the research focus in recent decades, which has been predominantly on emitters in the visible spectral range [3]. As a consequence, the technology of semiconductor-based UV emitters indicates a high optimization potential, which could open up numerous use-cases in the field of medical and industrial applications [4]. In contrast to conventionally used gas discharge lamps, semiconductor emitters offer the possibility of narrow-band spectra across the entire UV range, allowing

The associate editor coordinating the review of this manuscript and approving it for publication was Jiajie Fan.

This work is licensed under a Creative Commons Attribution 4.0 License. For more information, see https://creativecommons.org/licenses/by/4.0/

chemical or biological processes to be selectively excited [5], [6]. Due to the fast time response of the semiconductors and the direct dependence on electrical operating parameters, a temporal modulation of the radiation sources can be performed [7], which could induce additional effects in the irradiated samples. Furthermore, the spatial radiation characteristics of the radiation sources can be selectively adjusted to realize an areal irradiation in a compact design space. Alternatively, spot focusing allows locally selective excitation of photochemical reactions.

The emitters of the ultraviolet spectral range can be processed by using composite crystals based on the binary III-V-compound semiconductors InN, AlN and GaN [8]. UV LEDs below 360 nm are primarily designed with $Al_{1-x}Ga_xN$-based quantum wells, indicating a predominantly single-digit external quantum efficiency due to high defect density and low extraction efficiency [9]. In addition, the high defect density causes a significant degradation of the semiconductor structures, leading to a reduction in optical power of more than 30 % within the first 1000 hours of operation [10], [11].

For UV-A semiconductor emitters with a peak emission wavelength above 360 nm, the quantum wells are based on $In_{1-x}Ga_xN$. As a result, the external quantum efficiency can be quantified between 40 - 50 % depending on the device structure and design [12]. Due to the low indium content in the quantum wells, the energetic band offset between the quantum wells and the barriers could be small (energetic offset in conduction band ΔE_c and valence band $\Delta E_v \approx 0.15$ eV), promoting an escape of excited carriers from the active region [13].

Furthermore, photons generated within the active region could be absorbed in surrounding GaN layers of the semiconductor structure, significantly reducing the radiant flux of the device [14]. As a consequence, the reduced efficiency results in an increased self-heating of the semiconductor structure affecting the lifetime of the emitters [13].

Unlike the numerous publications analyzing the degradation behavior of blue and phosphor-converted LEDs, only a few papers were published regarding the degradation mechanisms and behavior of $In_{1-x}Ga_xN$-based UV-A LEDs [13], [15], [16], [17], [18], [19], [20], [21]. Compared directly with emitters of the blue spectral range, a significantly shorter lifetime of ultraviolet or near-ultraviolet structures can be observed [3]. The decrease in optical power can be caused by the formation of point defects, which can be traced back to previously studied GaN defects such as gallium vacancies, nitrogen antisite defects, or carbon impurities [13]. Additionally, energetic ultraviolet photons could provoke degradation mechanisms in the packaging of the semiconductor devices. Especially silicone encapsulated emitters are exposed to package-related degradation, occurring by yellowing or cracking of the silicone lens [15], [17]. As a result, the ultraviolet emitters can be expected to undergo a variety of possible aging mechanisms, which can be observed in both the LED's package and the semiconductor's structure significantly affecting the lifetime of the device [21].

To describe the occurrence of aging mechanisms and their effect on optical power loss, it seems obvious to use established lifetime modeling approaches for LEDs of the visible spectral range. These models forx luminous flux depreciation have been investigated in numerous studies and became standardized. Therefore, the Illuminating Engineering Society of North America (IES) recommends to perform LED lifetime projections on aging data collected under conditions described in the LM-80-20 standard [22]. By defining stress test conditions, measurement intervals and test methods, a harmonization of data collection should be ensured. Subsequent lifetime predictions are performed using the standardized methods described in TM-21-19 [23]. Respectively, an exponential function is fitted to the dataset collected for a LM-80 stress test period of more than 6000 h. According to TM-21-19, the projection of current or temperature conditions not covered by LM-80 conditions, is achieved by interpolations between the exponential fits using linear functions or the Arrhenius equation. To account for scenarios in which the degradation dynamics cannot be described by the typical exponential TM-21 function, supplementary mathematical approaches are provided in the standard. However, for these supplementary functions, inter- and extrapolations between different temperature conditions or operating currents are not given. To mitigate such weaknesses of the standard, additional approaches were introduced in literature [24], [25] e.g. double exponential functions [26], [27] or modified logarithmic functions [11].

In addition to simplified curve fitting methods, stochastic methods were established allowing to get probabilistic estimates regarding the device lifetime with variable aging parameters e.g. the IEC 62717:2014 standard [28], Gamma process models [29], [30], [31], Wiener process models [32], Filter and Brownian motion process approaches [33], [34].

Since LM-80 stress tests have to be performed for more than 6000 hours, accelerated test procedures have been developed [34], [35], [36]. These accelerations allow a significant reduction of total testing time and thus their accompanying costs. By performing the tests with higher operating conditions, the degradation mechanisms are expected to be accelerated and thus, a calculation to normal operating conditions can be performed.

Mechanisms accelerated by temperature are typically modeled using the Arrhenius equation [37]. Additional aging parameters, such as current, can be taken into account by Black's equation, which was initially developed to describe the process of electromigration in semiconductors [38], [39]. Therefore, the time to failure (TTF) is given by the two assumed independent variables of junction temperature T_j and stress current I_a using

$$TTF(T_j, I_a) = K \cdot \exp\left[\frac{E_a}{k_B T_j}\right] \cdot I_a^{-n}. \quad (1)$$

Model parameters such as activation energy E_a, exponent n and coefficient K can be determined by using stress test data collected at different current and temperature conditions, whereas k_B correspondents to the Boltzmann constant. Another possibility of accelerated lifetime modeling is given by the Eyring model [39]. The model allows a consideration of thermal and several non-thermal factors and their interactions, but it's not considered in depth for the modeling part of this publication.

Due to the small number of available reports discussing the degradation behavior of emitters of the violet/ultraviolet spectral range, the degradation dynamics and the physical degradation mechanisms of silicon-encapsulated LEDs with a peak wavelength of 365 nm are analyzed within the scope of this work. We identified the photon-induced silicon lens cracking as the main lifetime limiting process for cost-effective 365 nm emitters, and modeled the emitters' TTF and the Safe Operating Area (SOA) for a wide range of operating conditions by using Black's equation. The reported results could help to identify potential device optimizations, which could be considered for future generations of UV-A emitters.

II. EXPERIMENTAL SETUP AND SAMPLES

The experiments were carried out on commercially available UV-A high-power LEDs with a rated peak wavelength of 365 nm at 350 mA. At this operating point the external quantum efficiency of the devices can be quantified with 46 %. The acquired devices had very low manufacturing tolerances in terms of forward voltage, I-V characteristics and electro-optical efficiency, so no pre-selection of devices was made. Typical device characteristics can be found in Table 1.

TABLE 1. Overview of device characteristics at a measurement current of 350 mA. The values given are mean values from 32 devices with associated standard deviations.

Peak-wavelength (nm)	Radiant flux (W)	Forward voltage (V)	Electrical power (W)	Degradation time (hours)
366.0 ±0.2	0.539 ±0.014	3.68 ±0.04	1.237 ±0.014	8665

To perform the stress tests, the silicone-encapsulated surface mount devices were assembled on a metal core printed circuit board each. In order to analyze the effect of forward current and temperature on device degradation, the thermal structure functions of the samples were determined with a thermal impedance measurement system (T3ster - Mentor Graphics).

Taking into account the thermal resistances, two different test designs were realized. An iso-thermal test design was used to draw conclusions about the effect of forward current at approximately identical junction temperatures. Therefore, three different forward currents were applied to the devices (350 mA, 500 mA, 700 mA) and the junction temperature was set to $T_j = 100\,°C$ with an assumed uncertainty of ±4 K. The estimation of the temperature uncertainty results as a worst-case estimate, affected by the measurement of the thermal resistance, the absolute radiant flux and the temperature coefficient k. Consequently, the uncertainty is to be considered as an expanded measurement uncertainty ($p = 95.4\,\%$).

To study the effect of temperature at constant forward current ($I_a = 350\,mA$) the devices' case temperatures were varied. The stress test conditions and the determined junction temperatures result according to Table 2. For each aging condition, four samples were stressed for a test period of 8665 hours. Furthermore, additional groups of four samples were stressed in a temperature chamber at junction temperatures of $T_j = 105\,°C$ and $T_j = 132\,°C$.

TABLE 2. Selected test conditions for the performed stress test.

	Stress current I_a (mA)	Junction temperature T_j ±4 K (°C)
Temperature plate	350	70, 100, 115, 130
	500	100
	700	100
Temperature chamber	350	105
	700	132

The absolute maximum ratings specified by the manufacturer are given with a junction temperature of $T_j = 90\,°C$ and a maximum forward current of $I_f = 700\,mA$. The aging conditions were selected within and above the manufacturer's specification. It should be noted, that some stress conditions were deliberately chosen above the maximum ratings to evaluate an acceleration of the provoked aging mechanisms.

The stress tests were carried out on separate temperature-controlled heating plates, whose temperatures were controlled measuring the LED boards' T_c points. The ambient conditions of these plates were set to room temperature with 25 °C and a relative humidity of $RH = 30\,\%$. During aging the characterization of the samples was performed by disassembling the LED boards from the heating plates and performing a measurement at a dedicated LED measurement system, which has been described in detail in previous publications [40], [41].

The optical measurements were carried out using a spectroradiometer (CAS140CT - Instrument Systems) in combination with an integrating sphere (PTFE 30 cm). The system is absolutely calibrated and provides information of the electroluminescence (EL) spectrum and the absolute emitted spectral radiant flux. Measurements above 1 mA were carried out pulsed to reduce joule-heating within the active region. The spectroradiometers' integration time was set to 10 ms, with a current pulse width of 15 ms. Due to the fact that a pulsed current of 15 ms could cause effects of joule-heating, the integration time and pulse width was kept constant for the entire stress test period allowing to assume a systematic error in radiant flux. During the measurement, the LED's solderpoint temperature was controlled by a peltier element in combination with a peltier controller (ITC 4020 - Thorlabs).

To study the operating point dependent degradation of the structures, the spectrum was taken at nine different forward

currents. A current-voltage characteristic taken at each measurement interval, extends the dimensions of degradation mechanism analysis.

III. RESULTS AND DISCUSSION

A. DEGRADATION MECHANISMS

In the following, the physical degradation mechanisms of silicone-encapsulated UV-A LEDs are analyzed before their dependence on aging conditions is evaluated. The degradation behavior shown in Fig. 1 is representative for the samples stressed at a junction temperature of $T_j = 70\,°C$ and a stress current of $I_a = 350\,mA$.

The results indicate measurement current dependent degradation mechanisms. With decreasing measurement current the effect of optical power loss increases, resulting in a reduction of 40 % in optical power at $I_m = 1\,mA$ and a stress current of $I_a = 350\,mA$. In addition, an increase in radiant flux above its initial value can be observed for all measurement currents within the first 26 hours of operation. The process is followed by a gradual optical power loss that persists throughout the entire stress test period. For low-injection currents, the gradual power loss indicates an increased slope in the log-log *OP-I* curves, not shown here.

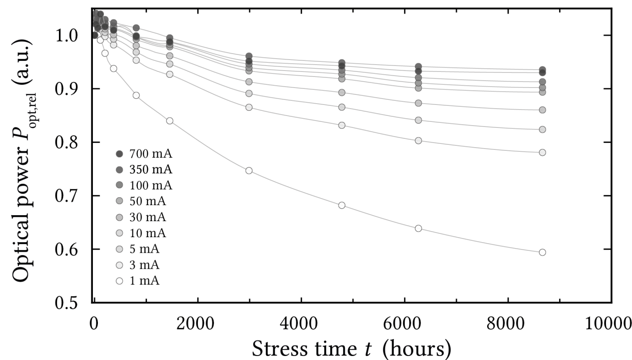

FIGURE 1. Reduction of optical power $P_{opt,rel}$ for different measurement currents I_m (normalized to the value at 0 h) for a period of 8665 hours. The degradation dynamics are representative for devices stressed at $T_j = 70\,°C$ and $I_a = 350$ mA.

Taking into account the electrical properties of the emitters, the previously described increase in optical power is accompanied by several changes in the current-voltage characteristics.

The characteristics shown in Fig. 2 can be divided in three sections. Section I represents the low-injection regime, indicating a voltage drop within the first measurement interval. The initial decrease is followed by a slower but gradual increase in parasitic conduction mechanisms, primarily affecting the low-injection regime. Operating points in section II and III (I_f >0.5 mA) are driven by competing mechanisms. For forward currents in section II (0.5 mA < I_f < 100 mA) an analogous, but less intense initial voltage drop is observed, indicating a maximum at 30 mA. The changes within the first measurement interval are highlighted in Fig. 3. Section II indicates a voltage drop, which

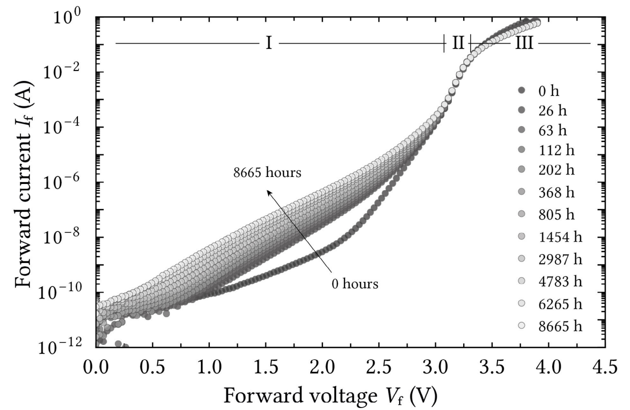

FIGURE 2. Semi-logarithmic current-voltage characteristics of one representative sample operated at $T_j = 70\,°C$ and $I_a = 350$ mA.

is separated from the initial drop in the low-injection regime. The inset in Fig. 3 shows a local maximum of forward voltage reduction for $I_m = 30\,mA$, whereas the transition between low- and high-injection regime (0.5 mA) remains unaffected.

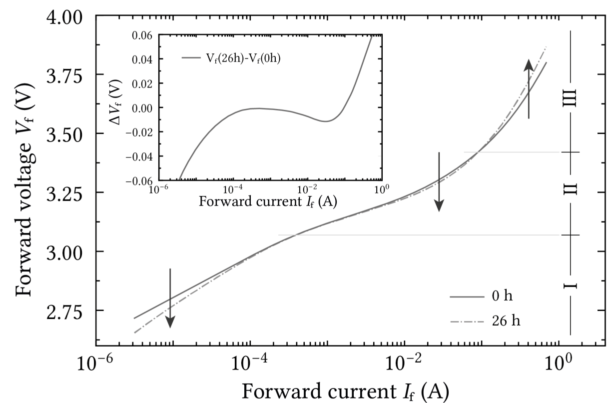

FIGURE 3. Semi-logarithmic voltage-current characteristics of one representative sample operated at $T_j == 70\,°C$ and $I_a = 350$ mA before stress and after 26 h of operation. Inset: Forward voltage difference inferred from the data before and after 26 h of stress.

The time-dependent forward voltage for $I_m = 30\,mA$, shown in Fig. 4, indicates the initial voltage reduction being counteracted in the following. By considering the series resistance (section III) and its temporal behavior, superimposed effects by two competing mechanisms become apparent. For operating points in section III ($I_f > 100\,mA$) a gradual voltage increase is observed, being primarily affected by an increase in series resistance.

Analyzing the radiant flux depreciation in detail, a square root time dependence can be identified for $t > 26$ h, shown in Fig. 5. The dependence is also present for all operating points not shown here. Taking into account the time dependence of the determined ideality factor n_{ideal}, inferred from the measurement data by using the methods described in [42], an analogous behavior can be identified. Therefore, n_{ideal} drops within the first measurement interval from 1.79 to

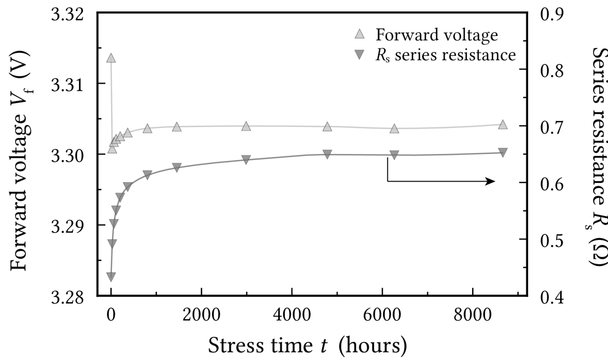

FIGURE 4. Forward voltage measured at $I_m = 30$ mA and differential series resistance for 8665 hours of stress at $T_j = 70\,°C$ and $I_a = 350$ mA.

1.70 and increases gradually with a square root time dependence to 1.86. As a result the optical power $P_{opt,rel}$ and the ideality factor n_{ideal} can be described for $t > 26$ h by

$$P_{opt,rel}(t) = P_{opt,rel}(26) + m_{opt,rel} \cdot \sqrt{t} \quad (2)$$

and

$$n_{ideal}(t) = n_{ideal}(26) + m_{ideal} \cdot \sqrt{t}, \quad (3)$$

respectively. Derived from the slopes shown in Fig. 5 $m_{opt,rel}$ and m_{ideal} can be determined. Due to the square root time dependence of ideality factor and the radiant flux decrease, a linear correlation between these characteristics can be inferred.

Examining the LED package, no degradation of the silicone encapsulation can be detected, manifested by a constant peak wavelength, not shown here.

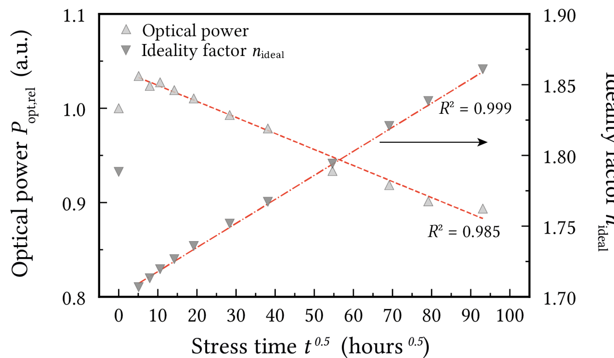

FIGURE 5. Normalized optical power at $I_m = 30$ mA and ideality factor at $V_f = 3.179$ V as a function of the square root of time.

Based on the previously presented results, the degradation of the devices can be separated in two modes:

I.) The initial increase of radiant flux accompanied by a forward voltage decrease can be attributed to an Mg acceptor activation in the p-side. The higher conductivity of the p-type region, increased hole injection efficiency and reduced Schottky-barrier at the p-contact result in an increase of optical radiant flux within the first 26 hours of operation [43], [44]. In particular, the increased hole injection efficiency leads to an increase in optical power, affecting all investigated operating points equally. Synchronously, the low-injection regime indicates an increase of point defects in and around the active region [45]. These point defects could act as non-radiative recombination centers and promote parasitic conduction mechanisms by trap-assisted tunneling processes (TAT). Especially the current-voltage characteristics shown in Fig. 2 indicate increasing parasitic currents in the low-injection regime, that could be promoted by TAT. As the defects become saturated with higher current density, operating points above $I_f = 1$ mA are primarily affected by Mg acceptor activation. In this range, the resulting voltage drop increases linear with forward current and reaches a maximum at 30 mA, not shown here. Operating points above 30 mA are primarily driven by an increase of series resistance, becoming the dominant mechanism at higher operating currents.

II.) The subsequent degradation for $t > 26$ h is characterized by a gradual decrease in radiant flux indicating a square root time dependence. In addition, the ideality factor and forward currents in the low-injection regime also show a comparable degradation dynamics. According to various literatures, such dependencies suggests diffusion processes to be involved [44], [46], [47], [48], [49], [50], [51]. Hydrogen or Mg-dopant atoms migrate from p-doped layers to the active region resulting in an increase of non-radiative recombination accompanied by parasitic current paths. In violet LEDs stressed by Nam et al. [52] a magnesium back diffusion from the p-doped layers was observed, indicated by a broadening of the initial doping profiles. The diffusion of Mg atoms into the active region was suggested to be the major mechanism for optical power loss. Moreover, the diffusion of Mg is much more pronounced in LEDs grown on sapphire substrate compared to layers grown on free-standing GaN, suggesting that dislocations promote the diffusion of point defects. Nevertheless, it should be noted that the exponential radiant flux decrease observed by Nam et al. does not coincide with the square root dependent results shown in Fig. 5. Additionally, the observed Mg diffusion processes have never been confirmed by other studies. In high current density experiments ($3\,kA\,cm^{-2}$) performed on InGaN laser diodes, no significant change in the Mg concentration profile was observed [53].

Therefore, the migration of hydrogen accompanied by a de-hydrogenation of V_{Ga}-H_3 defect complexes seems to be a more appropriate explanation for the generation of point defects within the active region [44].

As a result of the manufacturing process, the hydrogen concentration follows the magnesium profile in the p-doped layers. The incorporated hydrogen passivates both acceptors and negatively charged point defects. Various studies in (In)AlGaN LEDs revealed a hydrogen diffusion from the p-doped layers to the n-side during operation, leaving behind negatively charged point defects [44], [54]. Such point defects could act as non-radiative recombination centers and assist parasitic conduction mechanisms in the low-injection

regime. According to Nykänen et al. [55], the required energy to remove hydrogen atoms from V_{Ga}-H_n defect complexes in GaN is 1 eV. Studies by Van de Walle et al. [56] locate the energy required for de-hydrogenation between 2 eV and 3.25 eV.

Consequently, different interactions can be considered for the removal of H from V_{Ga}-H_n defect complexes:

a.) Temperature-induced activation of defects: Considering a junction temperature of $T_j = 70\,°C$ a thermal energy of 29.5 meV can be assumed, allowing to rule out a temperature-driven de-passivation of the defects.

b.) Interaction with hot carriers: According to Iveland et al. [57], the kinetic energy spectrum of electrons in InGaN LEDs shows a local maximum at 2 eV, supporting a de-hydrogenation of the defects by collisions with hot carriers. Due to the correlation between optical power decay and the inverse of the cube of the stress current density Ruschel et al. [11] proposed Auger recombinations to be involved in the generation of hot carriers in 310 nm UV-B LEDs.

c.) Auger-driven recombination: Recent studies [58], [59], [60], [61] suggest a new type of Auger-driven recombination process. The process is different from classical Auger recombination due to its dependence on trap concentration. As a result of its quadratic dependence on carrier density and its relation with defect density, this process could drive the degradation of optoelectronic GaN structures. Since this recombination mechanism has been proposed recently, its effect on optical power depreciation has not been fully investigated [61].

d.) Photo-induced effects: Results presented by De Santi et al. [62] demonstrated the formation of point defects in irradiated InGaN LEDs using a 405 nm laser and an irradiance of 361 W cm^{-2}. Similar results were reported by Caria et al. [63] in open-circuit conditions. Consequently, it should be considered that V_{Ga}-H_n defect complexes could also be de-hydrogenated by the energetic short wavelength radiation (365 nm $\approx$ 3.4 eV).

Accordingly, a possible scenario is the V_{Ga}-H_n defect complex de-hydrogenation by interactions with hot electrons, defect-assisted Auger recombinations or energetic photons [64]. The separated hydrogen atoms diffuse to the n-side and leave behind negatively charged point defects, explaining both the optical and electrical degradation of the emitters.

Due to the partial linear correlation between low-injection forward current increase at e.g. 2.62 V (1 µA) and optical power loss, a direct link between defects promoting trap-assisted tunneling processes and non-radiative recombinations centers affecting the high-injection regime could be suggested.

The negatively charged point defects left behind in the p-side would result in acceptor decompensation, explaining the increase in series resistance. Since the change of the series resistance deviates from the square root dependence of radiant flux depreciation, it can be assumed that the change of R_s is driven by additional mechanisms. Although the previously described diffusion of Mg atoms would result in a change of the forward voltage, comparable degradation dynamics between R_s and P_{opt} would be expected.

These deviations could be explained by a worsening of metal/semiconductor interface at the p-type region, described by Meneghini et al. [65]. As a result of hydrogen diffusion from the passivation layer to the immediate proximity of the p-contact Mg acceptors are passivated, whereas acceptors of the bulk remain unaffected. Therefore, the reduced conductivity of the Schottky contact seems a plausible origin of different electrical and optical degradation dynamics being observed in the high-injection regime.

In conclusion, it is not possible to identify the underlying gradual degradation mechanisms in detail, rather, promising scenarios are presented likely explaining the observed device behavior.

Above junction temperatures of $T_j = 70\,°C$, the silicone encapsulated packages indicate crack formation within the primary lens, shown in Fig. 6.

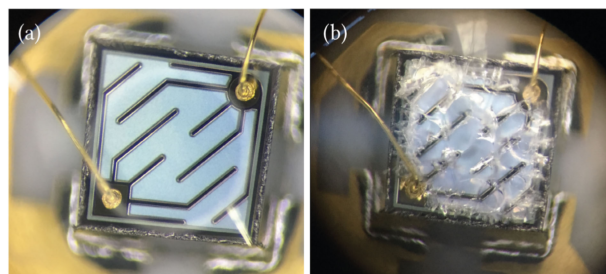

FIGURE 6. LED chip with silicone lens before (a) and after stress test (b) at T_j = 100 °C and I_a = 350 mA.

For an aging current of $I_a = 350$ mA and a junction temperature $T_j = 100\,°C$ (beyond maximum rating), the decrease in optical power for different measurement currents, results according to Fig. 7. Within the first 1700 hours of operation, the degradation behavior is comparable to devices without lens cracking. After crack formation, the measured optical power reduces significantly and an increase in the peak wavelength of $\Delta\lambda_p = 0.5$ nm can be observed, not shown here.

Based on the aging data, it can be concluded that lens cracking is followed by a progression of crack formation, successively contributing to a step wise reduction of the radiant flux. In detail, the observed crack formation affects the reduction of optical power to a different extend, varying with measurement current. A change in the light extraction efficiency η_{extr} is expected to decrease the optical power uniformly at all operating points, assuming that no current dependence of η_{extr} is given [40].

Fig. 8 shows the external quantum efficiency for different measurement currents. Under the premise that the operating point at $I_m = 700$ mA is exclusively affected by a reduction in light extraction efficiency (LEE), the red dashed decrease

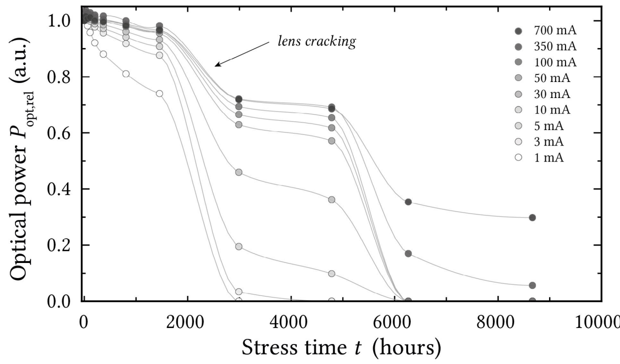

FIGURE 7. Reduction of optical power $P_{\text{opt,rel}}$ for different measurement currents I_{m} (normalized to the value at 0 h) for a period of 8665 hours. The degradation dynamics are representative for devices stressed at $T_{\text{j}} = 100\,^{\circ}\text{C}$ and $I_{\text{a}} = 350$ mA.

should result. Consequently, measurement currents below 700 mA are affected by an additional aging mechanism that accompanies crack formation and does not only affect light extraction efficiency.

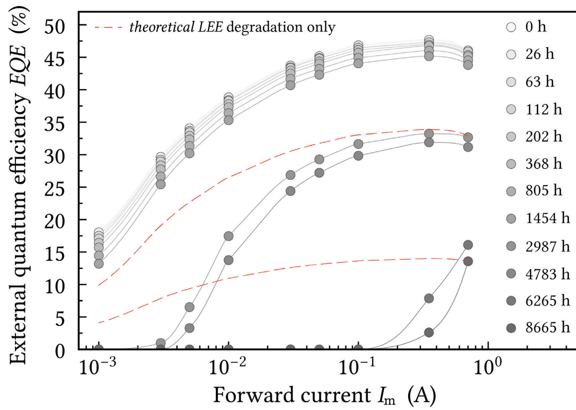

FIGURE 8. Change in current-dependent external quantum efficiency for a representative device with crack formation in the primary lens. The degradation of an exclusive change of extraction efficiency is shown dashed.

According to Fig. 8, the further progression of the crack formation manifests that the decrease of the external quantum efficiency after 8665 hours cannot be exclusively explained by a change of transmission properties of the silicone lens.

A better understanding of the device degradation can be achieved under consideration of the current-voltage characteristic shown in Fig. 9. The abrupt change in forward voltage observed here, occurs synchronously with crack formation and suggests an additional electrical degradation mechanism of the device. The additional process is characterized by the formation of a parasitic conductive path shorting the active region. With stress time the conductivity increases and indicates, due to its logarithmic progression in Fig. 9, an ohmic behavior. After 8665 hours of stress, the effect of the reduced parallel resistance R_{p} dominates almost all operating points of the electrical characteristic.

By removing the silicone lens, the chip surface can be assessed. Fig. 10 (a) shows the chip surface representative

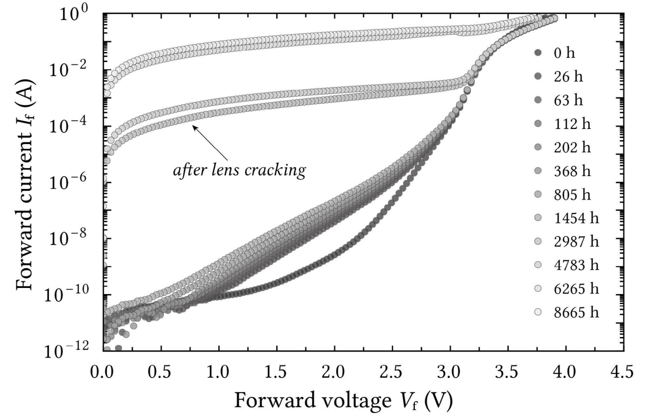

FIGURE 9. Semi-logarithmic current-voltage characteristics of one representative sample operated at $T_{\text{j}} = 100\,^{\circ}\text{C}$ and $I_{\text{a}} = 350$ mA.

for the stressed devices. The highlighted area is close to the electrical contacts and indicates surface damage in the indium tin oxide (ITO) layer. The additional image of the structure under forward bias with $I_m = 350\,\text{mA}$ confirms a lower luminescence of the device, which is accompanied by an inhomogeneous emission in the lateral chip dimension.

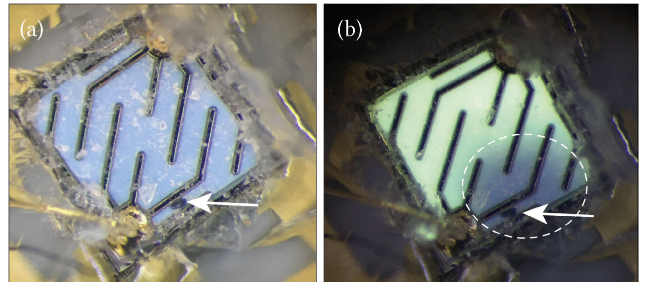

FIGURE 10. Exposed chip surface of damaged device with crack formation. Damage to the ITO layer can be seen in the area of the electrical contacts (a). Identical device at forward-bias with $I_{\text{m}} = 350$ mA (b). The area around the defect of the ITO layer shows a significantly lower luminescence.

In particular, the area around the defect shown in Fig. 10 (a) suffers from a lower radiance, indicating a significant current flow within the device. Thus the electrical degradation, which occurs synchronously with crack formation, contributes primarily to the decrease in optical power.

Crack formation within the primary lenses can be attributed to bond breaking and embrittlement of the polydiphenylsiloxane used for the LED's encapsulation [66]. While covalent Si-O bonds have an average binding energy of 4.6 eV and thus can only be dissociated with radiation in the UVC range, the Si-C bonds have a binding energy of 3.17 eV and can interact with photons of a wavelength below 391 nm [67], [68]. The removal of the phenyl groups (-C_6H_5) is followed by the formation of new Si-O bonds, which is expected to result in stronger cross-linking of the silicone, accompanied by the embrittlement of the material [66]. The lower elasticity of the encapsulant and the deviating thermal expansion coefficient

compared to the semiconductor chip leads to the formation of cracks within the primary lens and could promote delamination processes of the silicone encapsulant from the chip surface [69], [70]. Disassembling and cooling down the devices for optical and electrical characterization favors the accumulation of moisture in the previously formed cracks and delaminated areas of the silicone encapsulant. Switching on the devices after measurement leads to an abrupt expansion of accumulated moisture and thus, expands the prevailing cracks. Therefore, temperature/power cycling is crucial for this type of crack formation. Furthermore, the higher reflection at the material interfaces and a higher absorption within the encapsulant result in a stronger self-heating of the silicone, additionally accelerating the embrittlement.

For the devices studied, the metallic n-contacts are located on top of the semiconductor structure placed on a layer of indium tin oxide (ITO) [21]. According to Singh et al., the formation of ohmic conduction mechanisms is due to the migration of metal atoms into the active region [71]. The origin of the metal atoms can be both, the electrical contacts and the ITO layer itself [72]. A diffusion of moisture, oxidizing substances and corrosive gases through the silicone lens could result in a dissolved ITO layer by electrolytic corrosion. Therefore, with the appearance of the lens cracking the underlying passivation layer becomes vulnerable. Possible effects of delamination accompanying the process of lens cracking could affect the fraction of moisture prevailing at the chips' surface. Emerging electrolytic corrosions separate metallic indium migrating through a damaged passivation layer, finally shorting the active region. The increasing conductivity of the ohmic leakage channel shown in Fig. 9, is due to the ongoing chemical reduction of ITO, resulting in an agglomeration of metallic indium atoms at the leakage path. The self-heating of the resulting shunt accelerates the degradation of the device itself.

In conclusion, the degradation of the silicone encapsulated UV-A LEDs in this temperature range is due to the occurrence of radiation-induced cracks in the primary lens, which is followed by processes of electromigration. The extent to which the device temperature and the forward current contribute to an acceleration of these degradation mechanisms will be discussed in the following.

B. TEMPERATURE DEPENDENCY OF DEGRADATION MECHANISMS

The temperature dependency of the degradation mechanisms and the associated reduction of optical power for 8665 hours of stress is shown in Fig. 11. With increasing junction temperature, the time to failure is reduced, indicating a significant temperature dependence of the catastrophic failure. In addition, further embrittlement of the silicone and electromigration after cracking is temperature dependent, manifested by a faster reduction of optical power with increasing temperature. Temperature acceleration of gradual optical degradation caused by defect generation within the semiconductor can only be analyzed to a limited extent, especially

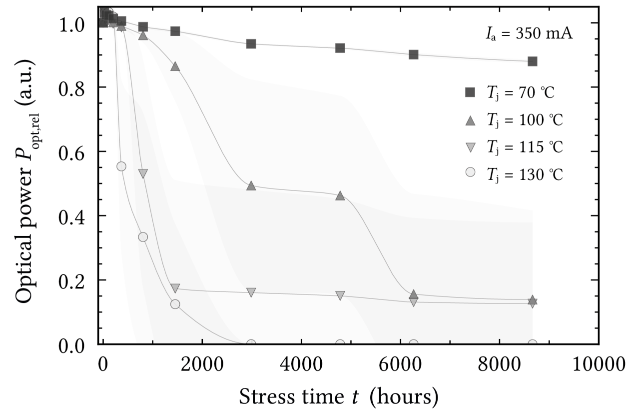

FIGURE 11. Decrease in optical power $P_{opt,rel}$ measured at $I_m = 30$ mA for different case temperatures $T_j = 70\,°C$, $100\,°C$, $115\,°C$ and $130\,°C$ at stress current $I_a = 350$ mA. Mean values with associated standard deviation (shades).

since the degradation is dominated by lens cracking and the accompanying processes of electromigration.

Defining the occurrence of crack formation as failure criterion of the device, the averaged lifetime results according to Fig. 12. Depending on junction temperature, there is an exponential decrease in time to failure, that could be described using the reciprocal Arrhenius equation. The occurrence of the failure criterion TTF as a function of junction temperature T_j is obtained using

$$TTF(T_j) = C \cdot \exp\left[\frac{E_a}{k_B T_j}\right] \tag{4}$$

with activation energy E_a, Boltzmann constant k_B and coefficient C.

According to Fig. 12 an activation energy of 0.8 ± 0.2 eV can be determined. The resulting coefficient of determination $R^2 = 0.99$ indicates an adequate representation of the degradation mechanism using the Arrhenius equation.

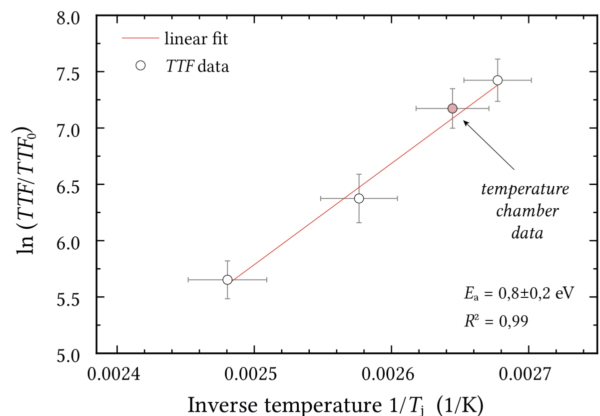

FIGURE 12. Logarithmic *TTF* versus inverse junction temperature with standard deviations at $I_a = 350$ mA. Additional data from the temperature chamber is shown, stressed at $I_a = 350$ mA and $T_j = 105\,°C$.

Due to the activation energy of 0.8 ± 0.2 eV, a strong temperature dependence of the polymer embrittlement can

be concluded, which has already been analyzed in various studies [69]. Significantly lower activation energies have been determined for general lighting white LEDs (0.2 eV-0.5 eV) [72]. The chemical processes within the siloxane encapsulant are accelerated with temperature and thus the degradation of the primary lens. Despite the different processes and reactions occurring within the materials, the occurrence of the failure criterion can be described accurately using the Arrhenius equation.

C. CURRENT DEPENDENCY OF DEGRADATION MECHANISMS

For a junction temperature of $T_j = 100\,°C$ and three forward currents of 350 mA, 500 mA and 700 mA the current dependent decrease of radiant flux results according to Fig. 13. Analogous to the degradation at different junction temperatures, all samples exhibit embrittlement of the primary lens accompanied by an electrical degradation of the structures. According to Fig. 13 the process of crack formation, defined as a failure criterion, is accelerated with current density. For a forward current of 700 mA, the *TTF* occurs after about 531 ± 168 hours, whereas a lifetime of 1675 ± 546 hours can be observed at 350 mA. The stated uncertainties result from the time intervals between the measurements and must therefore be assumed to be distributed uniformly. The isothermal test design allows to conclude that the degradation is primarily accelerated by radiant flux coupled into the primary lens causing a stronger crosslinking of the siloxane. Within the operating conditions considered, the radiant flux increases almost linearly with forward current.

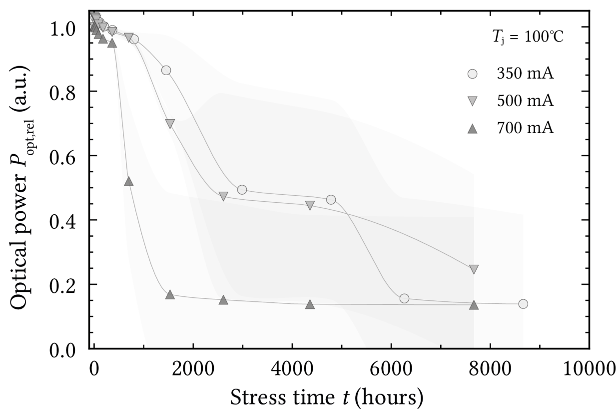

FIGURE 13. Decrease in optical power $P_{opt,rel}$ measured at $I_m = 30$ mA for different stress currents $I_a =$ 350 mA, 500 mA and 700 mA at $T_j = 100\,°C$. Mean values with calculated standard deviation (shades).

The non-thermal accelerated degradation can be described using the inverse power law, whereas the time to failure is calculated as a function of aging current I_a with

$$TTF(I_a) = D \cdot I_a^{-n}. \tag{5}$$

Using a linearizing transformation, the exponent n can be determined from the slope of the dependencies shown in Fig. 14.

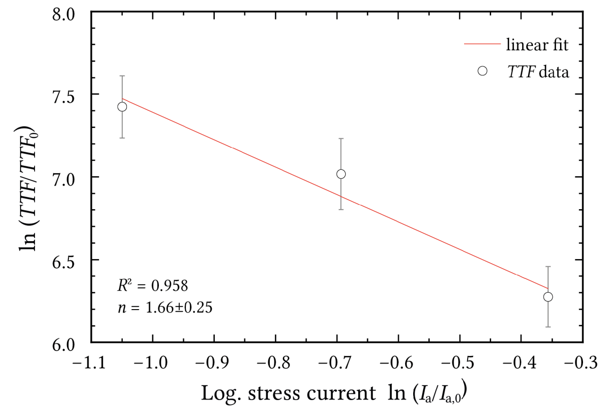

FIGURE 14. Logarithmic *TTF* with standard deviation versus logarithmic stress current I_a.

The coeffcient D is also determined by the previously mentioned curve fitting. Based on the measurement data, this results in $n = 1.66$ and $D = 306$, giving the current-dependent lifetime in hours

$$TTF(I_a) = 306 \cdot I_a^{-1.66}. \tag{6}$$

Despite the fact that the transformed lifetimes can only be described to a limited extent using a linear curve fit, it must be taken into account that an equal distribution can be assumed within the uncertainty intervals. Consequently, a linear regression can be considered as appropriate.

In direct comparison with LEDs of the visible spectral range, it must be noted that general lighting white LEDs indicate n values between −0.15 to 2.89, whereas activation energies between 0.07 eV and 0.34 eV are determined [72]. The large variation of these parameters is attributed to different device packages and thus dominant degradation mechanisms. Due to a missing phosphor layer in ultraviolet LEDs and shorter emission wavelength, different aging mechanisms occur compared to white LED packages. As a result, the determined activation energies and n coefficients differ from existing studies based on white mid- and high-power LEDs.

D. LIFETIME MODELLING

Considering the dominance of primary lens embrittlement and crack formation, the modeling of gradual semiconductor degradation is obsolete unless a working range can be defined within no damage to the silicone encapsulant is to be expected. The definition of crack formation as a failure criterion allows the modeling of the lifetime of the silicone encapsulant and thus of the entire semiconductor device. Based on the measurement data collected at different aging conditions, a lifetime model is derived, allowing to calculate the *TTF* in dependence of stress current and temperature. In addition, the operating range of the LEDs could be defined using the model equation, whereby no crack formation of the primary lens is to be expected for a defined time interval.

The lifetime model is based on Black's equation and therefore on a multiplication of temperature AF_T and current

dependent AF_I acceleration factors, with

$$AF_T = \frac{TTF_{\text{ref}}}{TTF_{\text{acc}}} = \exp\left[\frac{E_{\text{a}}}{k_{\text{B}}}\left(\frac{1}{T_{\text{j,ref}}} - \frac{1}{T_{\text{j,acc}}}\right)\right] \tag{7}$$

and

$$AF_I = \frac{TTF_{\text{ref}}}{TTF_{\text{acc}}} = \left(\frac{I_{\text{a,acc}}}{I_{\text{a,ref}}}\right)^n, \tag{8}$$

resulting in

$$AF = AF_T \cdot AF_I \tag{9}$$

and

$$AF = \exp\left[\frac{E_{\text{a}}}{k_{\text{B}}}\left(\frac{1}{T_{\text{j,ref}}} - \frac{1}{T_{\text{j,acc}}}\right)\right] \cdot \left(\frac{I_{\text{a,acc}}}{I_{\text{a,ref}}}\right)^n. \tag{10}$$

Alternatively, the lifetime can be calculated using

$$TTF(T_{\text{j}}, I_{\text{a}}) = K \cdot \exp\left[\frac{E_{\text{a}}}{k_{\text{B}} T_{\text{j}}}\right] \cdot I_{\text{a}}^{-n}. \tag{11}$$

The coefficient K is calculated from the quotient of the previously determined coefficient C and the aging current of the different temperature conditions $I_{\text{a,Temp}}$ using $K = C/I_{\text{a,Temp}}^{-n}$. A surface plot of the dependencies described in 11 is shown in Fig. 15, indicating that the operating parameters of the devices have to be limited due to the degradation processes in the primary lens.

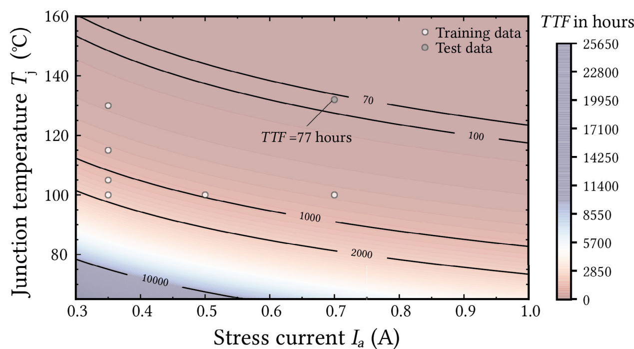

FIGURE 15. Surface plot of the device lifetime as a function of stress conditions I_{a} and T_{j} with contour lines. The data points used for model generation are shown with white markers, while the validation of the model is performed using the data set shaded in dark gray.

Using the surface diagram shown above, the lifetime can be determined as a function of operating parameters.

According to Fig. 15, a lifetime of more than 10000 hours can only be expected for a small range of aging conditions. Therefore the LEDs should ideally be operated below $T_{\text{j}} = 65\,°\text{C}$ and $I_{\text{a}} = 350\,\text{mA}$.

The maximum junction temperature T_{j}, which should not be exceeded to reach a defined lifetime TTF, is obtained as a function of aging current by

$$T_{\text{j}} = \frac{E_{\text{a}}}{k_{\text{B}}} \cdot \left(\ln\left(\frac{TTF \cdot I_{\text{a}}^n}{K}\right)\right)^{-1}. \tag{12}$$

In order to validate the model derived from the measurement data shown in Fig. 15, an additional data set is analyzed with respect to its consistency with the model prediction. The test data set is gathered analogous to the previously used aging data, and therefore the measured lifetime represents the average of four individual samples. For an aging current of $I_{\text{a}} = 700\,\text{mA}$ and a junction temperature of $T_{\text{j}} = 132\,°\text{C}$, a lifetime of $TTF = 75 \pm 25$ hours is measured. The model predicts a value of 77 hours, which allows to conclude that the occurrence of the failure mechanism can be modeled within the boundaries of the considered operating range.

For the aging condition at $I_{\text{a}} = 350\,\text{mA}$ and $T_{\text{j}} = 70\,°\text{C}$ no cracking of the primary lens occurs after 8665 hours of stress. The lifetime model predicts a TTF of 14730 hours, thus a continuation of the tests allows an additional validation of the model. An overview of the measured TTF and the corresponding model prediction is given in Table 3.

TABLE 3. Comparison of measured ***TTF*** and model prediction for different operating conditions.

Stress current I_{a} (mA)	Junction temperature T_{j} ±4 K (°C)	Test results hours	Model prediction hours
350	70	> 8665	14730
350	100	1675 ± 546	1702
350	105	1305 ± 396	1228
350	115	587 ± 219	655
350	130	285 ± 85	271
500	100	1116 ± 531	943
700	100	531 ± 168	540
700	132	75 ± 25	77

To evaluate the effect of temperature/power cycling due to the electro-optic characterizations, two additional devices were stressed for an interval of 300 hours at $T_{\text{j}} = 132\,°\text{C}$ and $I_{\text{a}} = 700\,\text{mA}$. The characterizations and optical inspections were carried out before stress and after 300 hours of operation. In contrast to regularly measured devices under identical conditions (expected TTF =75 h), no visible crack formation in the primary lens could be observed for the entire period. Therefore, it could be stated that temperature/power cycling accompanied by a process of moisture diffusion is crucial to initiate the effect chain of visible crack formation and subsequent electromigration.

In summary, the temperature dependence of crack formation can be described using the Arrhenius equation, while the current-induced acceleration can be modeled using the inverse power law. Using the combined equation of the dependencies, also known as Black's equation, the TTF can be modeled in the analyzed operating range. The validity of the model is demonstrated with an additional data set.

To which extent the validity of the model equation can be guaranteed beyond the operating range, cannot be assessed on the basis of the current data situation. Additional data sets, currently measured at $I_{\text{a}} = 350\,\text{mA}$ and $T_{\text{j}} = 70\,°\text{C}$, are located within the model prediction and do not show any damage in the primary lens so far. In addition, it remains to be considered that the model is valid for the aging conditions and measurement protocols used. Avoiding temperature/power cycles for characterizations will lead to deviating

device lifetimes. Similar effects are also expected for deviations in relative humidity, significantly affecting degradation dynamics [73]. As a result, the validity of the model should be assumed exclusively for the conditions and measurement protocols used.

IV. CONCLUSION

Based on the analyzed data of silicone encapsulated UV-A LEDs, we conclude that the lifetime of the devices is affected by aging processes within the semiconductor structures as well as by package-related degradation mechanisms. The generation of point defects within the semiconductor structure is accompanied by radiation-induced crack formation in the primary lens. Occurring lens cracks are enhanced by temperature/power cycling due to the performed measurements, finally promoting processes of electromigration shorting the active region. The processes are accelerated by increasing thermal and electrical stress parameters, whose dependencies can be described by the Arrhenius equation and the inverse power law. A multiplicative combination of the functional dependencies, also known as Black's equation, allows lifetime and SOA modeling, the validity of which could be confirmed with independently collected data sets. The failure mechanisms studied in the stress tests can be used by manufacturers and research groups to optimize future generations of ultraviolet devices with regard to their lifetime and reliability. To separate the observed aging mechanisms, additional experiments will be carried out on identical devices without encapsulant.

ACKNOWLEDGMENT

The work reported in this paper reflects the author's view and that the JU is not responsible for any use that may be made of the information it contains.

REFERENCES

[1] L. Y. Kuritzky, C. Weisbuch, and J. S. Speck, "Prospects for 100% wall-plug efficient III-nitride LEDs," *Opt. Exp.*, vol. 26, no. 13, pp. 16600–16608, Jun. 2018.
[2] P. Kusuma, P. M. Pattison, and B. Bugbee, "From physics to fixtures to food: Current and potential LED efficacy," *Horticulture Res.*, vol. 7, no. 1, pp. 1–9, Dec. 2020.
[3] A. B. M. H. Islam, D.-S. Shin, and J.-I. Shim, "Enhanced radiative recombination rate by local potential fluctuation in InGaN/AlGaN near-ultraviolet light-emitting diodes," *Appl. Sci.*, vol. 9, no. 5, p. 871, Feb. 2019.
[4] N. Trivellin, F. Piva, D. Fiorimonte, M. Buffolo, C. De Santi, V. T. Orlandi, F. Dughiero, G. Meneghesso, E. Zanoni, and M. Meneghini, "UV-based technologies for SARS-CoV2 inactivation: Status and perspectives," *Electronics*, vol. 10, no. 14, p. 1703, Jul. 2021.
[5] C.-K. Huang and J.-G. Sung, "The application of UV-LEDs to microlithography," in *Proc. Int. Conf. Integr. Commercialization Micro Nanosyst.*, vol. 42940, 2008, pp. 579–582.
[6] L. Huang, H. Liao, J. Yang, and Z. Zeng, "Synthesis and properties of new UVA-sensitive photoacid generators of super acid for near-UV LED applications," *J. Photochem. Photobiology A, Chem.*, vol. 367, pp. 124–127, Dec. 2018.
[7] E. F. Schubert, N. E. J. Hunt, R. J. Malik, M. Micovic, and D. L. Miller, "Temperature and modulation characteristics of resonant-cavity light-emitting diodes," *J. Lightw. Technol.*, vol. 14, no. 7, pp. 1721–1729, Jul. 1996.
[8] H. Amano, R. Collazo, C. De Santi, S. Einfeldt, M. Funato, J. Glaab, S. Hagedorn, A. Hirano, H. Hirayama, R. Ishii, and Y. Kashima, "The 2020 UV emitter roadmap," *J. Phys. D, Appl. Phys.*, vol. 53, no. 50, Dec. 2020, Art. no. 503001.
[9] M. Kneissl and J. Rass, *III-Nitride Ultraviolet Emitters*. Berlin, Germany: Springer, 2016, pp. 10–13.
[10] H. Xiu, Y. Zhang, J. Fu, Z. Ma, L. Zhao, and J. Feng, "Degradation behavior of deep UV-LEDs studied by electro-optical methods and transmission electron microscopy," *Current Appl. Phys.*, vol. 19, no. 1, pp. 20–24, Jan. 2019.
[11] J. Ruschel, J. Glaab, B. Beidoun, N. L. Ploch, J. Rass, T. Kolbe, A. Knauer, M. Weyers, S. Einfeldt, and M. Kneissl, "Current-induced degradation and lifetime prediction of 310 nm ultraviolet light-emitting diodes," *Photon. Res.*, vol. 7, no. 7, p. B36, 2019.
[12] M. Kumar, "Advances in UV-A and UV-C LEDs and the applications they enable," in *Proc. SPIE*, vol. 10940, Mar. 2019, Art. no. 1094008.
[13] D. Monti, M. Meneghini, C. De Santi, G. Meneghesso, and E. Zanoni, "Degradation of UV-A LEDs: Physical origin and dependence on stress conditions," *IEEE Trans. Device Mater. Rel.*, vol. 16, no. 2, pp. 213–219, Jun. 2016.
[14] E. F. Schubert, *Light-Emitting Diodes*, 3rd ed. Troy, NY, USA: E. Fred Schubert, 2018, pp. 244–245.
[15] F. J. Arques-Orobon, N. Nuñez, M. Vazquez, C. Segura-Antunez, and V. González-Posadas, "High-power UV-LED degradation: Continuous and cycled working condition influence," *Solid-State Electron.*, vol. 111, pp. 111–117, Sep. 2015.
[16] I.-H. Lee, A. Y. Polyakov, S.-M. Hwang, N. M. Shmidt, E. I. Shabunina, N. A. Tal'nishnih, N. B. Smirnov, I. V. Shchemerov, R. A. Zinovyev, S. A. Tarelkin, and S. J. Pearton, "Degradation-induced low frequency noise and deep traps in GaN/InGaN near-UV LEDs," *Appl. Phys. Lett.*, vol. 111, no. 6, Aug. 2017, Art. no. 062103.
[17] B. Liang, Z. Wang, C. Qian, Y. Ren, B. Sun, D. Yang, Z. Jing, and J. Fan, "Investigation of step-stress accelerated degradation test strategy for ultraviolet light emitting diodes," *Materials*, vol. 12, no. 19, p. 3119, Sep. 2019.
[18] F. J. Arques-Orobon, M. Vazquez, and N. Nuñez, "Lifetime analysis of commercial 3 W UV-A LED," *Crystals*, vol. 10, no. 12, p. 1083, Nov. 2020.
[19] V. T. Shamirzaev, V. A. Gaisler, and T. S. Shamirzaev, "Edge and defect luminescence of powerful ultraviolet InGaN/GaN light-emitting diodes," *Semiconductors*, vol. 50, no. 11, pp. 1493–1498, Nov. 2016.
[20] T. Mukai, D. Morita, M. Yamamoto, K. Akaishi, K. Matoba, K. Yasutomo, Y. Kasai, M. Sano, and S. Nagahama, "Investigation of optical-output-power degradation in 365-nm UV-LEDs," *Phys. Status Solidi C*, vol. 3, no. 6, pp. 2211–2214, Jun. 2006.
[21] L.-R. Chen, S.-C. Huang, J.-L. Chiu, C.-C. Lu, W.-M. Su, C.-Y. Weng, H.-Y. Shen, T.-C. Lu, and H. Chen, "Degradation mechanisms of bias stress on nitride-based near-ultraviolet light-emitting diodes in salt water vapor ambient," *Microelectronic Eng.*, vol. 218, Oct. 2019, Art. no. 111158.
[22] *Approved Method: Measuring Luminous Flux and Color Maintenance of LED Packages, Arrays, and Modules, IES LM-80-20*, Illum. Eng. Soc. North America, New York, NY, USA, 2020.
[23] *Projecting Long Term Lumen Maintenance of LED Light Sources, IES TM-21–19*, Illuminating Eng. Soc. North America, New York, NY, USA, 2019.
[24] F.-K. Wang and Y.-C. Lu, "Useful lifetime analysis for high-power white LEDs," *Microelectron. Rel.*, vol. 54, nos. 6–7, pp. 1307–1315, Jun. 2014.
[25] L. Xu and K. Qian, "Aging mathematical model of InGaN/GaN LEDs based on non-radiative recombination," in *Proc. AIP Conf.*, 2017, Art. no. 020172.
[26] G. Bobashev, N. G. Baldasaro, K. C. Mills, and J. L. Davis, "An efficiency-decay model for lumen maintenance," *IEEE Trans. Device Mater. Rel.*, vol. 16, no. 3, pp. 277–281, Sep. 2016.
[27] W. D. Van Driel, M. Schuld, B. Jacobs, F. Commissaris, J. Van Der Eyden, and B. Hamon, "Lumen maintenance predictions for LED packages," *Microelectron. Rel.*, vol. 62, pp. 39–44, Jul. 2016.
[28] *Led Modules for General Lighting-Performance Requirements*, document IEC 62717, 2014.
[29] M. S. Ibrahim, J. Fan, W. K. C. Yung, Z. Wu, and B. Sun, "Lumen degradation lifetime prediction for high-power white LEDs based on the gamma process model," *IEEE Photon. J.*, vol. 11, no. 6, pp. 1–16, Dec. 2019.
[30] J. Fan, Y. Chen, Z. Jing, M. S. Ibrahim, and M. Cai, "A gamma process-based degradation testing of silicone encapsulant used in LED packaging," *Polym. Test.*, vol. 96, Apr. 2021, Art. no. 107090.

[31] Z. Wu, Z. Wang, Q. Feng, B. Sun, C. Qian, Y. Ren, and X. Jiang, "A gamma process-based prognostics method for CCT shift of high-power white LEDs," *IEEE Trans. Electron Devices*, vol. 65, no. 7, pp. 2909–2916, Jul. 2018.

[32] J. Huang, D. S. Golubovic, S. Koh, D. Yang, X. Li, X. Fan, and G. Q. Zhang, "Degradation modeling of mid-power white-light LEDs by using Wiener process," *Opt. Exp.*, vol. 23, no. 15, p. A966, 2015.

[33] P. Lall and J. Wei, "Prediction of L70 life and assessment of color shift for solid-state lighting using Kalman filter and extended Kalman filter-based models," *IEEE Trans. Device Mater. Rel.*, vol. 15, no. 1, pp. 54–68, Mar. 2015.

[34] J. Huang, D. S. Golubovic, S. Koh, D. Yang, X. Li, X. Fan, and G. Q. Zhang, "Lumen degradation modeling of white-light LEDs in step stress accelerated degradation test," *Rel. Eng. Syst. Safety*, vol. 154, pp. 152–159, Oct. 2016.

[35] S.-T. Tseng and Z.-C. Wen, "Step-stress accelerated degradation analysis for highly reliable products," *J. Quality Technol.*, vol. 32, no. 3, pp. 209–216, Jul. 2000.

[36] S. I. Chan, W. S. Hong, K. T. Kim, Y. G. Yoon, J. H. Han, and J. S. Jang, "Accelerated life test of high power white light emitting diodes based on package failure mechanisms," *Microelectron. Rel.*, vol. 51, nos. 9–11, pp. 1806–1809, 2011.

[37] L. Trevisanello, M. Meneghini, G. Mura, M. Vanzi, M. Pavesi, G. Meneghesso, and E. Zanoni, "Accelerated life test of high brightness light emitting diodes," *IEEE Trans. Device Mater. Rel.*, vol. 8, no. 2, pp. 304–311, Jun. 2008.

[38] R. L. De Orio, H. Ceric, and S. Selberherr, "Physically based models of electromigration: From black's equation to modern TCAD models," *Microelectron. Rel.*, vol. 50, no. 6, pp. 775–789, 2010.

[39] K.-Z. Tan, S.-K. Lee, and H.-C. Low, "LED lifetime prediction under thermal-electrical stress," *IEEE Trans. Device Mater. Rel.*, vol. 21, no. 3, pp. 310–319, Sep. 2021.

[40] A. Herzog, M. Wagner, and T. Q. Khanh, "Efficiency droop in green InGaN/GaN light emitting diodes: Degradation mechanisms and initial characteristics," *Microelectron. Rel.*, vol. 112, Sep. 2020, Art. no. 13792.

[41] A. Herzog, M. Wagner, and T. Q. Khanh, "Monitoring the optical degradation of green light-emitting diodes on the basis of measured electrical characteristics," *Microelectron. Rel.*, vol. 121, Jun. 2021, Art. no. 114147.

[42] D. Zhu, J. Xu, A. N. Noemaun, J. K. Kim, E. F. Schubert, M. H. Crawford, and D. D. Koleske, "The origin of the high diode-ideality factors in GaInN/GaN multiple quantum well light-emitting diodes," *Appl. Phys. Lett.*, vol. 94, no. 8, Feb. 2009, Art. no. 081113.

[43] C.-C. Liu, Y.-H. Chen, M.-P. Houng, Y.-H. Wang, Y.-K. Su, W.-B. Chen, and S.-M. Chen, "Improved light-output power of GaN LEDs by selective region activation," *IEEE Photon. Technol. Lett.*, vol. 16, no. 6, pp. 1444–1446, Jun. 2004.

[44] J. Glaab, J. Ruschel, T. Kolbe, A. Knauer, J. Rass, H. K. Cho, N. L. Ploch, S. Kreutzmann, S. Einfeldt, M. Weyers, and M. Kneissl, "Degradation of (In) AlGaN-based UVB LEDs and migration of hydrogen," *IEEE Photon. Technol. Lett.*, vol. 31, no. 7, pp. 529–532, Apr. 1, 2019.

[45] T. Yanagisawa, "Estimation of the degradation of InGaN/AlGaN blue light-emitting diodes," *Microelectron. Rel.*, vol. 37, no. 8, pp. 1239–1241, Aug. 1997.

[46] J. Glaab, C. Ploch, R. Kelz, C. Stölmacker, M. Lapeyrade, N. L. Ploch, J. Rass, T. Kolbe, S. Einfeldt, F. Mehnke, C. Kuhn, T. Wernicke, M. Weyers, and M. Kneissl, "Degradation of (InAlGa)N-based UV-B light emitting diodes stressed by current and temperature," *J. Appl. Phys.*, vol. 118, no. 9, Sep. 2015, Art. no. 094504.

[47] N. Renso, C. De Santi, A. Caria, F. D. Torre, L. Zecchin, G. Meneghesso, E. Zanoni, and M. Meneghini, "Degradation of InGaN-based LEDs: Demonstration of a recombination-dependent defect-generation process," *J. Appl. Phys.*, vol. 127, no. 18, May 2020, Art. no. 185701.

[48] C. De Santi, M. Meneghini, G. Meneghesso, and E. Zanoni, "Degradation of InGaN laser diodes caused by temperature- and current-driven diffusion processes," *Microelectron. Rel.*, vol. 64, pp. 623–626, Sep. 2016.

[49] C. H. Seager, S. M. Myers, A. F. Wright, D. D. Koleske, and A. A. Allerman, "Drift, diffusion, and trapping of hydrogen in *p*-type GaN," *J. Appl. Phys.*, vol. 92, no. 12, pp. 7246–7252, Dec. 2002.

[50] K. Orita, M. Meneghini, H. Ohno, N. Trivellin, N. Ikedo, S. Takigawa, M. Yuri, T. Tanaka, E. Zanoni, and G. Meneghesso, "Analysis of diffusion-related gradual degradation of InGaN-based laser diodes," *IEEE J. Quantum Electron.*, vol. 48, no. 9, pp. 1169–1176, Sep. 2012.

[51] I. S. Romanov, I. A. Prudaev, A. A. Marmalyuk, V. A. Kureshov, D. R. Sabitov, and A. V. Mazalov, "Effect of magnesium diffusion into the active region of LED structures with InGaN/GaN quantum wells on internal quantum efficiency," *Russian Phys. J.*, vol. 57, no. 4, pp. 533–535, Aug. 2014.

[52] O. H. Nam, K. H. Ha, J. S. Kwak, S. N. Lee, K. K. Choi, T. H. Chang, S. H. Chae, W. S. Lee, Y. J. Sung, H. S. Paek, and J. H. Chae, "Characteristics of GaN-based laser diodes for post-DVD applications," *Phys. Status Solidi A, Appl. Mater. Sci.*, vol. 201, no. 12, pp. 2717–2720, 2004.

[53] L. Marona, P. Perlin, R. Czernecki, M. Leszczynski, M. Bockowski, R. Jakiela, T. Suski, and S. P. Najda, "Secondary ions mass spectroscopy measurements of dopant impurities in highly stressed InGaN laser diodes," *Appl. Phys. Lett.*, vol. 98, no. 24, Jun. 2011, Art. no. 241115.

[54] J.-S. Park and K. J. Chang, "Diffusion and stability of hydrogen in Mg-doped GaN: A density functional study," *Appl. Phys. Exp.*, vol. 5, no. 6, Jun. 2012, Art. no. 065601.

[55] H. Nykänen, S. Suihkonen, L. Kilanski, M. Sopanen, and F. Tuomisto, "Low energy electron beam induced vacancy activation in GaN," *Appl. Phys. Lett.*, vol. 100, no. 12, Mar. 2012, Art. no. 122105.

[56] C. G. Van de Walle, "Interactions of hydrogen with native defects in GaN," *Phys. Rev. B, Condens. Matter*, vol. 56, no. 16, pp. 10020–10023, Oct. 1997.

[57] J. Iveland, L. Martinelli, J. Peretti, J. S. Speck, and C. Weisbuch, "Direct measurement of Auger electrons emitted from a semiconductor light-emitting diode under electrical injection: Identification of the dominant mechanism for efficiency droop," *Phys. Rev. Lett.*, vol. 110, no. 17, Apr. 2013, Art. no. 177406.

[58] A. David, N. G. Young, C. A. Hurni, and M. D. Craven, "Quantum efficiency of III-nitride emitters: Evidence for defect-assisted nonradiative recombination and its effect on the green gap," *Phys. Rev. A, Gen. Phys.*, vol. 11, no. 3, Mar. 2019, Art. no. 031001, doi: 10.1103/PhysRevApplied.11.031001.

[59] W. Liu, C. Haller, Y. Chen, T. Weatherley, J.-F. Carlin, G. Jacopin, R. Butté, and N. Grandjean, "Impact of defects on Auger recombination in C-plane InGaN/GaN single quantum well in the efficiency droop regime," *Appl. Phys. Lett.*, vol. 116, no. 22, Jun. 2020, Art. no. 222106, doi: 10.1063/5.0004321.

[60] A. C. Espenlaub, D. J. Myers, E. C. Young, S. Marcinkevicius, C. Weisbuch, and J. S. Speck, "Evidence of trap-assisted Auger recombination in low radiative efficiency MBE-grown III-nitride LEDs," *J. Appl. Phys.*, vol. 126, no. 18, Nov. 2019, Art. no. 184502, doi: 10.1063/1.5096773.

[61] M. Buffolo, A. Caria, F. Piva, N. Roccato, C. Casu, C. De Santi, N. Trivellin, G. Meneghesso, E. Zanoni, and M. Meneghini, "Defects and reliability of GaN-based LEDs: Review and perspectives," *Phys. Status Solidi (A)*, vol. 219, no. 8, Apr. 2022, Art. no. 2100727.

[62] C. De Santi, A. Caria, N. Renso, E. Dogmus, M. Zegaoui, F. Medjdoub, G. Meneghesso, E. Zanoni, and M. Meneghini, "Evidence of optically induced degradation in gallium nitride optoelectronic devices," *Appl. Phys. Exp.*, vol. 11, no. 11, Nov. 2018, Art. no. 111002.

[63] A. Caria, C. De Santi, M. Buffolo, G. Meneghesso, E. Zanoni, and M. Meneghini, "Photon-induced degradation of InGaN-based LED in open-circuit conditions investigated by steady-state photocapacitance and photoluminescence," *J. Appl. Phys.*, vol. 131, no. 4, Jan. 2022, Art. no. 043102.

[64] F. Piva, C. De Santi, M. Deki, M. Kushimoto, H. Amano, H. Tomozawa, N. Shibata, G. Meneghesso, E. Zanoni, and M. Meneghini, "Modeling the degradation mechanisms of AlGaN-based UV-C LEDs: From injection efficiency to mid-gap state generation," *Photon. Res.*, vol. 8, no. 11, pp. 1786–1791, Oct. 2020.

[65] M. Meneghini, L. Rigutti, L. R. Trevisanello, A. Cavallini, G. Meneghesso, and E. Zanoni, "A model for the thermal degradation of metal/(p-GaN) interface in GaN-based light emitting diodes," *J. Appl. Phys.*, vol. 103, no. 6, Mar. 2008, Art. no. 063703.

[66] T. Nagatomo and N. Miki, "Reduction of parasitic capacitance of a PDMS capacitive force sensor," *Micromachines*, vol. 9, no. 11, p. 570, Nov. 2018.

[67] P. Margaretha, "Chemie der kohlenstoffverbindungen," in *Chemie Für Mediziner*. Berlin, Germany: Springer, 2002, pp. 77–172.

[68] Y. Nagasawa and A. Hirano, "Review of encapsulation materials for AlGaN-based deep-ultraviolet light-emitting diodes," *Photon. Res.*, vol. 7, no. 8, pp. 55–65, 2019.

[69] M. Y. Mehr, A. Bahrami, W. D. Van Driel, X. J. Fan, J. L. Davis, and G. Q. Zhang, "Degradation of optical materials in solid-state lighting systems," *Int. Mater. Rev.*, vol. 65, no. 2, pp. 102–128, Feb. 2020.

[70] M. Wagner, A. Herzog, H. Ganev, and T. Q. Khanh, "LED aging acceleration—An analysis from measuring and aging data of 14,000 hours LED degradation," in *Proc. 12th China Int. Forum Solid State Lighting (SSLCHINA)*, Nov. 2015, pp. 75–78.
[71] P. Singh and C. M. Tan, "A review on the humidity reliability of high power white light LEDs," *Microelectron. Rel.*, vol. 61, pp. 129–139, Jun. 2016.
[72] W. D. Van Driel, X. Fan, and G. Q. Zhang, *Solid State Lighting Reliability Part 2*. Berlin, Germany: Springer, 2017, pp. 527–547.
[73] J. Huang, D. S. Golubovic, S. Koh, D. Yang, X. Li, X. Fan, and G. Zhang, "Rapid degradation of mid-power white-light LEDs in saturated moisture conditions," *IEEE Trans. Device Mater. Rel.*, vol. 15, no. 4, pp. 478–485, Dec. 2015.

ALEXANDER HERZOG received the B.Sc., M.Sc., and Ph.D. degrees in electrical engineering from the Technische Universität Darmstadt, in 2012, 2015, and 2020, respectively. He is currently a Postdoctoral Researcher and a research group Leader with the Laboratory of Adaptive Lighting Systems and Visual Processing, Technische Universität Darmstadt. His research interests include lifetime prediction, reliability analysis, digital twins of light-emitting diodes, temporal light artifacts, and spectral optimization of metameric spectra.

SIMON BENKNER was born in Siegen, Germany, in 1987. He received the B.Sc. and M.Sc. degrees in electrical engineering from the Technische Universität Darmstadt, Germany, in 2015 and 2017, respectively, where he is currently pursuing the Ph.D. degree with the Laboratory of Adaptive Lighting Systems and Visual Processing. He is also working as a Research Assistant with the Laboratory of Adaptive Lighting Systems and Visual Processing, Technische Universität Darmstadt. His research interest includes reliability analysis of light-emitting diodes by applying physical and data driven models to increase lifetime prediction accuracy. In addition, he is concluding research on smart lighting systems.

BABAK ZANDI received the M.Sc. and Doctoral degrees in electrical engineering from the Technical University of Darmstadt. Currently, he is a research group Leader with the Laboratory of Adaptive Lighting Systems and Visual Processing, Darmstadt. He deals with various psychophysical and statistical methods to carry out and analyze investigations in automotive lighting. His research interests include the integration of neuronal networks in heuristic optimization procedures and the time- and spectral-dependent modeling of the human pupil light response. Further, he serves as an Editorial Board Member for *Scientific Reports*.

MATTEO BUFFOLO (Associate Member, IEEE) received the master's degree in electronic engineering from the University of Padova, in 2014, and the Ph.D. degree from the Department of Information Engineering, University of Padova, in March 2018. He is currently working as an Assistant Professor with the University of Padova. His research interests include the reliability of lighting systems employing GaN-based devices (lasers and LEDs) and the investigation of the degradation mechanisms that affect IR laser sources for integrated telecommunication applications.

WILLEM D. VAN DRIEL graduated the degree in mechanical engineering from the Technical University of Eindhoven, and the Ph.D. degree from the Delft University of Technology, The Netherlands. He has more than 25 years of track record in the reliability domain. Application areas range from healthcare, gas and oil explorations, and semiconductors. He is currently a Fellow Scientist with Signify (formerly Philips Lighting). Besides that, he holds a professor position with the University of Delft, The Netherlands. He has authored and coauthored more than 350 scientific publications, including, journals and conference papers, book or book chapters, and invited keynote lectures. His research interests include solid state lighting, microelectronics and microsystems technologies, virtual prototyping, virtual reliability qualification, and designing for reliability of microelectronics and microsystems. He is the Chair of the Organizing Committee of the IEEE Conference EuroSimE.

MATTEO MENEGHINI (Senior Member, IEEE) received the master's degree from the University of Padova, Padova, Italy, in 2004, and the Ph.D. degree in information engineering, working on the optimization of GaN-based LED and laser structures, from the University of Padova, in 2008. He is currently a Full Professor with the Department of Information Engineering, University of Padova, where he is involved in the electro-optical characterization and modeling of the performance and reliability of LEDs, lasers, HEMTs, and advanced solar.

TRAN QUOC KHANH received the Dr.-Ing. degree in physics and technology of electronic components and the Habilitation degree in mechanical engineering and technical optics from the Institute for Lighting Technology, Technische Universität Ilmenau, Germany, in 1989 and 2005, respectively. Since 2006, he has been a Full Professor and the Head of the Laboratory of Adaptive Lighting Systems and Visual Processing, Technical University of Darmstadt, where he has been serving as the Dean for the Department of Electrical Engineering and Information Technology, since 2018. He leads research groups in the field of automotive lighting, human-centric lighting, smart indoor lighting, and LED technology.